Bioactive Materials 48 (2025) 400–413

Contents lists available at ScienceDirect

Bioactive Materials

journal homepage: www.keaipublishing.com/en/journals/bioactive-materials

Precision repair of zone-specific meniscal injuries using a tunable extracellular matrix-based hydrogel system

Se-Hwan Lee [a,d], Zizhao Li [a,b], Ellen Y. Zhang [a,b], Dong Hwa Kim [a], Ziqi Huang [c], Yuna Heo [a], Sang Jin Lee [c], Hyun-Wook Kang [d], Jason A. Burdick [b,e], Robert L. Mauck [a,b,f], Su Chin Heo [a,b,f,*]

[a] McKay Orthopaedic Research Laboratory, Department of Orthopaedic Surgery, Perelman School of Medicine, University of Pennsylvania, Philadelphia, PA, 19104, United States
[b] Department of Bioengineering, School of Engineering and Applied Science, University of Pennsylvania, Philadelphia, PA, 19104, United States
[c] Biofunctional Materials, Division of Applied Oral Sciences and Community Dental Care, Faculty of Dentistry, The University of Hong Kong, 34 Hospital Road, Sai Ying Pun, Hong Kong SAR, PR China
[d] Department of Biomedical Engineering, Ulsan National Institute of Science and Technology, Ulsan, 44919, Republic of Korea
[e] BioFrontiers Institute and Department of Chemical and Biological Engineering, University of Colorado Boulder, Boulder, CO, 80309, United States
[f] Translational Musculoskeletal Research Center, Corporal Michael J Crescenz VA Medical Center, Philadelphia, PA, 19104, United States

ARTICLE INFO

Keywords:
Meniscus repair
Fetal/adult extracellular matrix
Methacrylated hyaluronic acid (MeHA)
Stiffness tunable hydrogel

ABSTRACT

Meniscus injuries present significant therapeutic challenges due to their limited self-healing capacity and the diverse biological and mechanical properties across the tissue. Conventional repair strategies do not replicate the complex zonal characteristics within the meniscus, resulting in suboptimal outcomes. In this study, we introduce an innovative fetal/adult and stiffness-tunable meniscus decellularized extracellular matrix (DEM)-based hydrogel system designed for precision repair of heterogeneous, zonal-dependent meniscus injuries. By synthesizing fetal and adult DEM hydrogels, we identified distinct cellular responses, including that hydrogels with adult meniscus-derived DEM promote more fibrochondrogenic phenotypes. The incorporation of methacrylated hyaluronic acid (MeHA) further refined the mechanical properties and injectability of the DEM-based hydrogels. The combination of fetal and adult DEM with MeHA allowed for precise tuning of stiffness, influencing cell differentiation and closely mimicking native tissue environments. *In vivo* tests confirmed the biocompatibility of hydrogels and their integration with native meniscus tissues. Furthermore, advanced 3D bioprinting techniques enabled the fabrication of hybrid hydrogels with biomaterial and mechanical gradients, effectively emulating the zonal properties of meniscus tissue and enhancing cell integration. This study represents a significant advance in meniscus tissue engineering, providing a promising platform for customized regenerative therapies across a range of heterogeneous fibrous connective tissues.

1. Introduction

The region-specific composition and architecture of fibrous connective tissues, such as tendons, ligaments, and the meniscus, present significant challenges for effective repair and regeneration. These tissues are characterized by complex biochemical compositions and biomechanical properties that are not uniform, but rather vary across different regions [1,2]. For instance, a gradient of collagen types and the spatial distribution of proteoglycans endow different areas within the same tissue with distinct mechanical characteristics [3]. This complexity is further compounded by the presence of diverse cell types, each finely tuned to their specific microenvironment [4,5]. This zonal heterogeneity is essential for the proper function of these tissues, but also complicates the development of effective treatment strategies. As a consequence, a traditional 'one-size-fits-all' approach to implant design is likely to be ineffective, emphasizing the need for regenerative approaches that can

Peer review under the responsibility of KeAi Communications Co., Ltd.
* Corresponding author. Orthopaedic Surgery and Bioengineering University of Pennsylvania McKay Orthopaedic Research Laboratory 375A Stemmler Hall 3450 Hamilton Walk, Philadelphia, PA, 19104, United States.
E-mail address: heosc@pennmedicine.upenn.edu (S.C. Heo).

https://doi.org/10.1016/j.bioactmat.2025.02.013
Received 1 November 2024; Received in revised form 6 February 2025; Accepted 6 February 2025

be tuned to reflect the intricate variations in these native tissues.

The meniscus is an important example of a heterogeneous tissue, as the diversity in biochemical and biomechanical properties is crucial for knee joint biomechanics, facilitating load-bearing and uniform force distribution in the knee. Meniscal tears, often caused by congenital defects, degenerative changes, or sports-related factors, impact roughly 70 individuals per 100,000 annually [6] and often require surgical intervention due to the limited self-repair capacity of the tissue [7]. The meniscus is distinctly zonal: the outer (red-red) region is vascularized, harboring fibroblast-like cells and type-I collagen which imparts stiffness and durability to the tissue (Fig. 1a). This outer region is particularly stiff and resistant to tensile forces due to its robust collagen structure [4,8]. In contrast, the inner (white-white) region is avascular completely, populated by chondrocyte-like cells, and rich in type-II collagen and proteoglycans, with a more randomly organized collagen fiber network (Fig. 1a) [9]. The intermediate (red-white) zone serves as a transitional area, blending characteristics of both the outer and inner regions [10]. Moreover, these zonal differences necessitate repair strategies that are tuned to each zone: the outer zone has better healing potential due to its vascularity, while the inner zone poses a greater challenge for repair due to its avascularity [11].

Meniscus tears also exhibit significant heterogeneity and variety (e.g., location, direction), with common types including longitudinal, radial, and horizontal tears (Fig. 1b) [11]. These tears, each with their distinct shape, orientation, and affected zones, underscore the necessity for customized treatment strategies [12]. These strategies must be sensitive to the unique attributes of each tear type to optimize healing and restore knee functionality. Commonly employed techniques such as suturing and arthroscopic partial meniscectomy (APM) offer contrasting approaches [13]; suturing aims to preserve and mend the tissue, while APM involves excising the damaged segment [14]. Despite their widespread use, both methods exhibit notable shortcomings when confronting complex meniscus tears: suturing is often inadequate for complex tear patterns (e.g., radial tears) [15], and APM results in increased local contact pressures that contribute to more rapid joint degeneration or osteoarthritis [16]. This highlights a significant gap in clinical practice, pointing to the urgent need for more sophisticated, tailored therapeutic modalities that ensure effective healing and joint

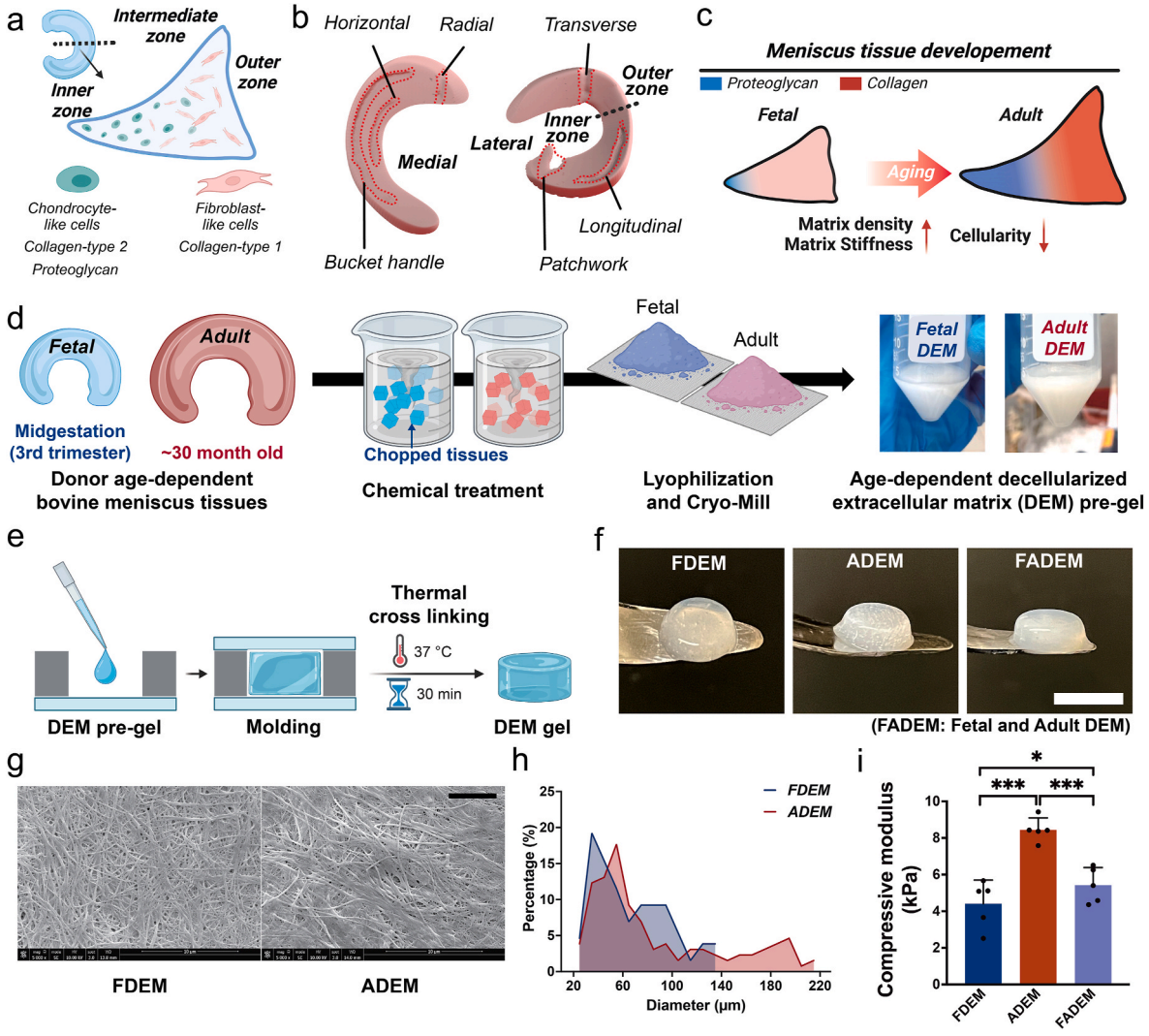

Fig. 1. Decellularization and Characterization of Fetal and Adult Meniscus Decellularized Extracellular Matrix (DEM) Hydrogels. Schematics showing a) heterogenous cell types and biochemical compositions across different meniscus zones, b) different types of meniscus tears that vary in direction and location, and c) biochemical alterations in meniscus tissue during development. Schematics of d) the SDS-based decellularization process to generate fetal and adult DEM hydrogel precursors (fetal: FDEM, adult: ADEM) and e) DEM hydrogel fabrication process using molding and thermal crosslinking. Characterization of DEM hydrogels, including f) images of fabricated DEM hydrogels (scale bar: 5 mm), g) field emission SEM images of the fibrous microstructure of DEM hydrogels (scale bar: 5 μm), h) fiber size distribution in FDEM and ADEM hydrogels, and i) compressive moduli of FDEM, ADEM, and their combination (FADEM) hydrogels (n = 5 per group; *p < 0.05, ***p < 0.001).

preservation.

Recently, decellularized extracellular matrix (DEM) systems have emerged as promising substrates for meniscus repair, offering a conducive microenvironment for cellular proliferation and tissue regeneration [17]. Yet, the challenge remains of effectively emulating the zonal-dependent properties and intrinsic heterogeneity of the meniscus using such systems. This challenge calls for innovative strategies that leverage DEM systems to mimic features of the distinct biochemical and biomechanical profiles of various zones in the meniscus. Therefore, the goal of this study was to engineer a tunable meniscus DEM-based hydrogel system that caters to the zonal specificity of meniscus tissue. By customizing the biochemical and mechanical properties of these hydrogels, we sought to mimic the native tissue characteristics of each meniscal zone. Moreover, the meniscus undergoes significant changes in protein composition and mechanical properties during development (Fig. 1c) [18]. This is evident when comparing fetal (from the midgestation, second and third trimester) and adult (from skeletally mature, 20–30 months) bovine menisci, which demonstrate an age-related increase in collagen and proteoglycan content from the inner to the outer zone [19]. Notably, donor age significantly influences tissue size and mechanical stiffness [20].

On this basis, here, we leveraged age-specific meniscus DEM — FDEM from fetal and ADEM from adult donors — to create biomimetic hydrogel systems. Our comprehensive biological characterizations revealed that the age-specific ECM components and mechanical properties of these hydrogels distinctly modulate meniscus cell behaviors and phenotypes. Building upon these insights, we furthered tuned the properties of DEM-based injectable hydrogel systems, by incorporating stiffness-tunable methacrylate hyaluronic acid (MeHA) [21], allowing precise control over hydrogel stiffness. MeHA also enhanced injectability and printability, expanding the potential routes for application of these hydrogels during surgical treatments. These advanced hydrogels, designed to mimic aspects of native ECM, offer promising zone-specific treatment strategies for fibrous connective tissue injuries, advancing tissue engineering and optimizing patient outcomes.

2. Results

2.1. Development and characterization of fetal and adult meniscus DEM hydrogels

Considering the influence of meniscal development on the biochemical and mechanical properties of the tissues [22], which in turn may subsequently affect cellular phenotypes, we first established a fetal and adult DEM system. This system utilizes bovine menisci from two distinct age groups (fetal: FDEM, adult: ADEM) to explore the regulatory effects of the fetal and adult meniscus ECM on cell behavior. Specifically, FDEM and ADEM from bovine tissue was generated through an SDS-based decellularization process (Fig. 1d). Post-decellularization, effective removal of the majority of cells was confirmed via DAPI and H&E staining (Supplementary Figs. S1a–d). Additionally, the preservation of collagen, a primary component of the meniscus, was validated through Picrosirius red staining (Supplementary Fig. S1e). Immunohistochemistry further confirmed that collagen type I and collagen type II were well preserved in both groups, while chondroitin sulfate proteoglycan, a key proteoglycan, was significantly more abundant in ADEM (Supplementary Fig. S1f).

Cylindrical DEM hydrogels (Diameter: 5 mm, Thickness: 2 mm) were produced using a molding method coupled with thermal crosslinking (Fig. 1e and f). Additionally, a composite group, FADEM, was created by combining FDEM and ADEM at a 1:1 ratio. Scanning electron microscopy (SEM) analysis verified the preservation of fibrous structures in both FDEM and ADEM hydrogels (Fig. 1g). Notably, ADEM hydrogels exhibited a broader fiber diameter distribution compared to FDEM hydrogels, likely reflecting developmental changes in ECM composition (Fig. 1h) [23]. The compressive modulus of the ADEM hydrogel (8.44 ± 0.65 kPa) was double that of the FDEM hydrogel (4.41 ± 1.29 kPa). Blending these two DEM types (FADEM) prior to gel formation (Fig. 1i) resulted in a compressive modulus (5.42 ± 0.96 kPa) that was intermediate to the FDEM and ADEM hydrogels alone. These distinctive features, including differences in fibrous structure and enhanced modulus, suggest that the age-related characteristics of native tissue are retained post-decellularization.

2.2. Impact of fetal and adult meniscus DEM on cell response

Based on our expectation of fetal and adult differences in the ECM of menisci that form these hydrogel systems, we hypothesized that these differences would translate into distinct cellular responses. Thus, we next explored how variations in the dECM composition, reflective of different developmental stages, affected cellular behavior, particularly in mesenchymal stem cells (MSCs) and meniscal fibrochondrocytes (MFCs). These cells, derived from juvenile bovine donors, are valuable resources in tissue engineering research due to their excellent proliferation, differentiation, and ECM production capabilities [24–26]. To do this, both cell types were first cultured on FDEM or ADEM hydrogels (Fig. 2a). MSCs cultured on ADEM hydrogels exhibited a large, more elongated cell morphology, while those on the FDEM hydrogel were notably smaller and more rounded (Fig. 2b–d, Supplementary Fig. S2a). MSCs on DEM hydrogels that combined features of both fetal and adult stages (FADEM) displayed intermediate morphologies. Similar trends were observed in MFCs under analogous conditions (Supplementary Figs. S3a–e), suggesting that the age-specific mechanical properties and biochemical cues of the DEM significantly influence cell morphology and phenotype across cell types.

To further assess cellular mechano-response, Yes-associated protein (YAP) nuclear localization, an indicator of mechanical activation of cells, was quantified [27]. In both FDEM and FADEM hydrogels, YAP was predominantly localized to the cytoplasm, whereas in the ADEM hydrogel, YAP was notably higher in the nucleus (Fig. 2b and e). This differential localization indicates distinct cellular responses to mechanical cues in their environment: nuclear YAP presence in the ADEM hydrogel suggests activation of pathways favoring fibrochondrocyte differentiation, essential for the load-bearing function of the outer meniscus [28–31], while cytoplasmic YAP in the FDEM and FADEM hydrogels may reflect a softer ECM that may promote chondrogenic differentiation [32–34].

Indeed, MSCs and MFCs both demonstrated significantly higher proliferation rates when cultured on the ADEM hydrogel (Fig. 2f and Supplementary Fig. S3f). Notably, FDEM hydrogel cultures exhibited a pronounced upregulation of chondrogenic markers, including Aggrecan (ACAN), SRY-Box Transcription Factor 9 (SOX9), and Transforming Growth Factor (TGF), while ADEM hydrogel cultures showed increased expression of fibrogenic markers including Collagen type I alpha 2 chain (Col1a2) in MSCs (Fig. 2g and h, Supplementary Fig. S2b). The ratio of the Col1a2 to Collagen type II (Col2) was elevated with the ADEM compared to FDEM hydrogel, suggesting a phenotype closer to fibrocartilage-like tissue in MSCs cultured on the ADEM hydrogel and chondrogenic tissue in MSCs cultured on the FDEM hydrogel [35]. The FADEM hydrogel presented intermediate characteristics in terms of cell proliferation and gene expression for both cell types (Fig. 2f–h and Supplementary Fig. S2b). Similarly, in MFCs, chondrogenic expression (e.g., ACAN, SOX9, and TGF) was upregulated for cells on FDEM hydrogels, while fibrogenic expression, including Col1a2 and Connective Tissue Growth Factor (CTGF), was more prominent for cells on ADEM hydrogels (Supplementary Fig. S3g).

2.3. Long-term assessment of age-specific meniscus DEM hydrogels in ex vivo models

Given that long-term stability and endogenous cell recruitment are crucial for successful tissue regeneration with hydrogels [36], we next

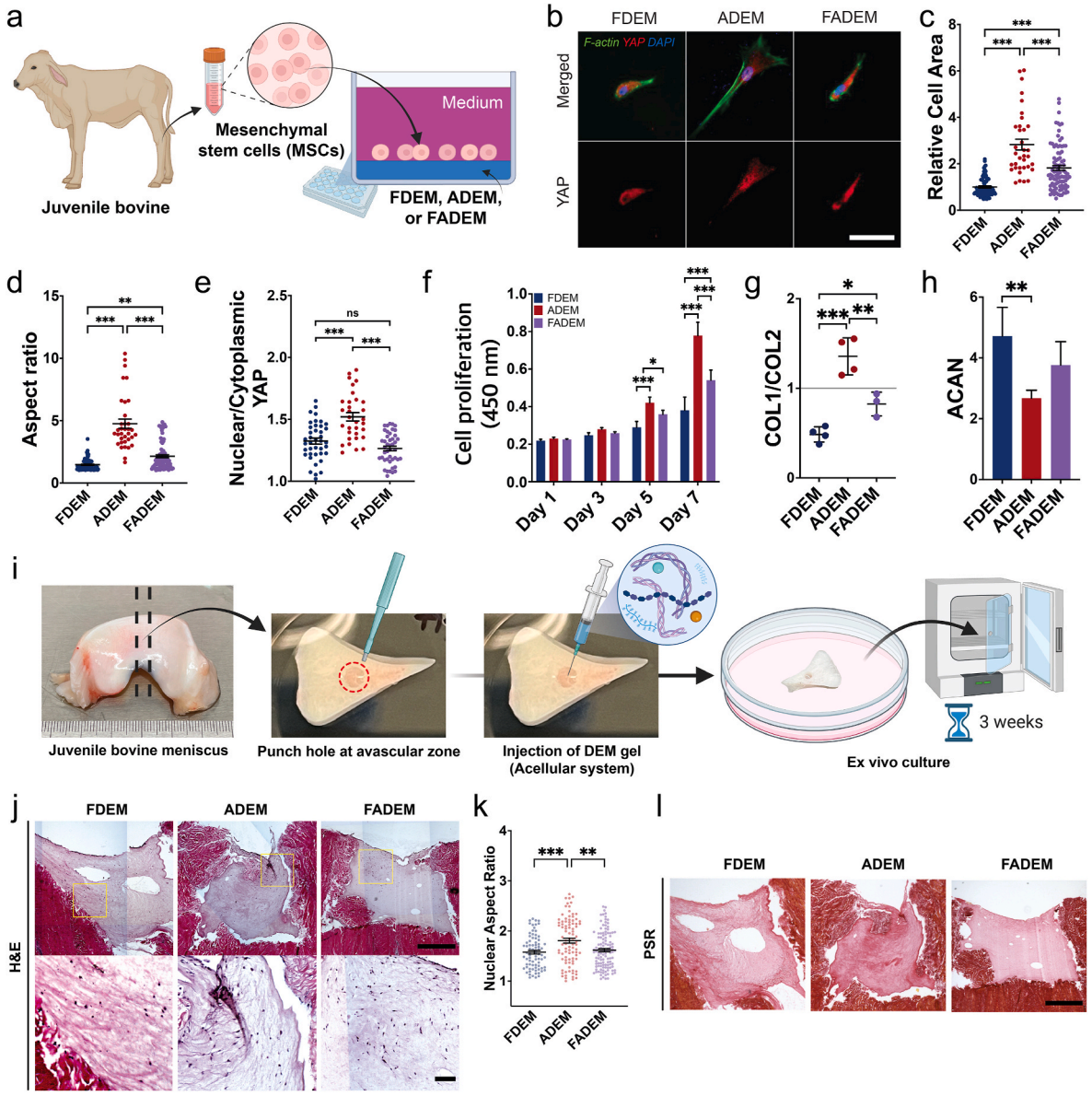

Fig. 2. Influence of Meniscus Age on Cellular Interactions with DEM hydrogels. a) Schematic of *in vitro* evaluation of cell response to DEM hydrogels from different ages (FDEM, ADEM, FADEM). Characterization of MSC interactions with DEM hydrogels at day 3, including b) representative images (Green: F-actin, Red: YAP, Blue: DAPI; Scale bar: 50 μm), c) relative cell area (n = 35–87), d) aspect ratio (n = 35–87), and e) YAP nuclear localization (n = 32–44). Characterization of MSCs with longer term culture on DEM hydrogels (for 7 days), including f) cell proliferation (n = 5) and g-h) gene expression (n = 3–4, COL1/COL2 and ACAN) (*p < 0.05, **p < 0.01, ***p < 0.001). i) Schematic of implantation and culture for 3 weeks of acellular DEM hydrogels within meniscus explants and outcomes, including j) representative H&E images [Scale bars: 750 μm (top) and 100 μm (bottom)], k) quantified nuclear aspect ratio of recruited cells (n = 67–118; **p < 0.01, ***p < 0.001), and l) representative picrosirius red stained images (Scale bar: 750 μm).

assessed the performance of the fetal and adult meniscus DEM hydrogels within a physiologically relevant environment. Specifically, we introduced acellular hydrogels into an ex-vivo meniscus defect model and incubated for three weeks (Fig. 2i). Hematoxylin and eosin (H&E) staining verified the preservation of FDEM, ADEM, and FADEM hydrogels throughout the incubation period, along with substantial cell infiltration from the surrounding native tissue (Fig. 2j). Consistent with our *in vitro* observations, cells migrating into the ADEM hydrogels exhibited more cell nuclei compared to those in other groups (Fig. 2j and k). All hydrogel types preserved their collagen composition, with ADEM hydrogels demonstrating more intense collagen staining (Fig. 2l). The persistence of collagen suggests that these hydrogels maintain their structural integrity over time, providing a stable scaffold conducive to tissue regeneration.

2.4. Proteomic analysis of fetal and adult DEM hydrogels reveals distinct biochemical composition

Given the observed differences in cellular responses to fetal and adult DEM hydrogel compositions and the known impact of tissue development on the biochemical composition of the meniscus [18], we performed proteomic analysis to investigate these differences. Samples were obtained from four fetal and adult meniscus donors, and subsequent principal component analysis (PCA) and heat map generation of detected proteins revealed minimal variability between individual donors, resulting in the formation of four distinct clusters (Fig. 3a and b, Supplementary Figs. S5a and b).

The analysis identified 1081 proteins in adult-derived DEM (ADEM) compared to 832 proteins in fetal-derived DEM (FDEM), indicating a more diverse and abundant array of proteins in ADEM (Fig. 3c). Post-

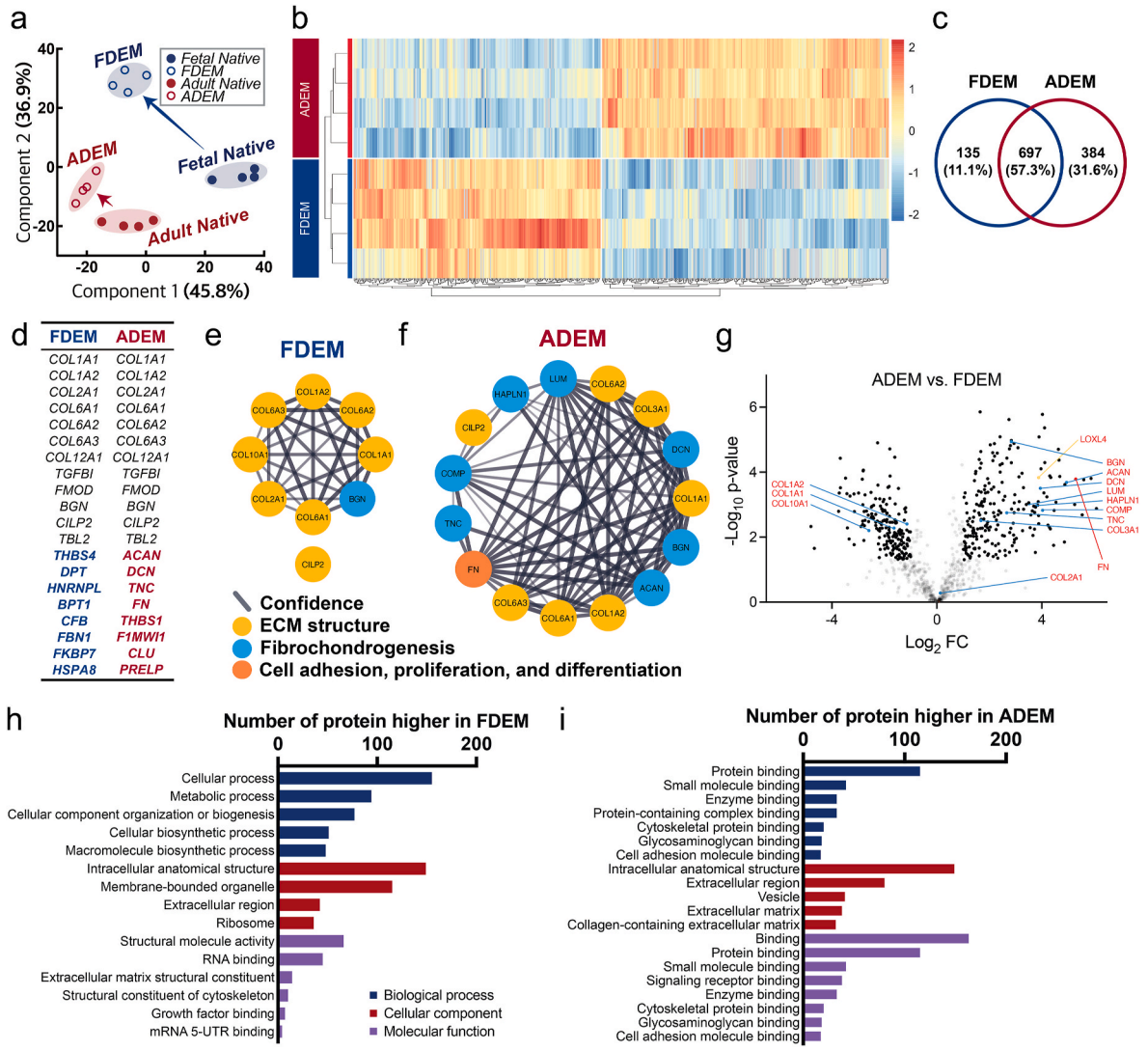

Fig. 3. Proteomic Analysis of Fetal and Adult Meniscus DEM. Proteomic analysis of FDEM and ADEM derived from four different donors per group, including a) principal component analysis (PCA) showing the distribution and variance of the protein composition, highlighting the distinct proteomic landscapes of FDEM and ADEM, b) heatmap and clusters of detected proteins, with clusters indicating the proteomic similarities and differences between the groups, c) Venn diagram depicting the overlap and unique proteins preserved in FDEM and ADEM, d) top 20 most prevalent proteins in FDEM or ADEM, Protein-protein interaction networks related to ECM structure, fibrochondrogenesis, cell adhesion, proliferation, and differentiation in (e) FDEM and (f) ADEM, with line thickness representing the confidence level of data support. g) Volcano plot of ADEM (vs. FDEM) visualizing the differentially expressed proteins between ADEM and FDEM, with statistical significance and fold-change metrics. Gene ontology analysis for biological process, cellular component, and molecular function in (h) FDEM and (i) ADEM showing the top 8 categories. (n = 4 per group from 4 differnt donors).

decellularization analysis confirmed the retention of several proteins integral to the native meniscus in both the FDEM and ADEM. These include Collagen Type-1 (COL1), Collagen Type-2 (COL2), Collagen Type-3 (COL3), Collagen Type-6 (COL6), Collagen Type-12 (COL12), Biglycan (BGN), and Cartilage Intermediate Layer Protein 2 (CILP2) (Fig. 3d and Supplementary Figure S5c). Notably, COL6 was abundant in both FDEM and ADEM. In addition to these structural proteins, our proteomic analysis revealed the presence of proteins associated with wound healing, regulatory functions, and ECM assembly. Proteins such as Transforming growth factor-beta-induced protein ig-h3 (TGFBI), Transducin beta like 2 (TBL2), and fibromodulin (FMOD) were abundant in both FDEM and ADEM (Fig. 3d) [37]. A more intriguing aspect revealed by proteomic analysis was the prevalence of fibrochondrogenic proteins in ADEM compared to FDEM. Fibrochondrogenic proteins such as Aggrecan (ACAN), Decorin (DCN), and Tenascin C (TNC) were more prevalent in ADEM than FDEM. Remarkably, Fibronectin (FN), a protein pivotal to cell adhesion and proliferation, was exclusively identified in ADEM group, where it exhibited significant interactions with other structural proteins, namely collagens (Fig. 3d–g). The retention of these major proteins post-decellularization suggests that essential components of native tissue are preserved after the process (Supplementary Figure S4).

In addition, a volcano plot further highlighted differentially abundant proteins in ADEM compared to FDEM, showing that proteins associated with fibrochondrogenesis (e.g., ACAN, DCN, and TNC) and cell adhesion (e.g., FN) were expressed at higher levels in ADEM than in FDEM (Fig. 3e). This differential expression likely contributes to the enhanced mechanical properties of ADEM hydrogels. Furthermore, Lysyl oxidase-like 4 (LOXL4), a protein implicated in collagen cross-linking [38] and fibrosis [39], was significantly upregulated in ADEM (Fig. 3e). These expression patterns align with those observed in native meniscus tissues (Supplementary Figs. S4d and e).

The abundance of cell adhesion-related proteins in ADEM may create a more favorable environment for cellular attachment to the structural

proteins compared to FDEM. This environment may encourage cells to adopt larger and elongated shapes, supporting cell proliferation and fibrochondrogenesis. The protein networks identified post-decellularization also form interconnected network structures similar to native tissue, potentially providing cells with a microenvironment that closely resembles the native ECM. Additional gene ontology (GO) analysis revealed that FDEM was enriched with proteins associated with cellular and metabolic processes, while ADEM exhibited a higher prevalence of proteins associated with protein or ECM binding (Fig. 3h, i and Supplementary Figs. S5a and b). Notably, GO analysis identified ADEM as being enriched in proteins related to cytoskeletal protein binding and cell adhesion molecule binding (Fig. 3i). The GO categories in DEM hydrogels closely align with those in native tissues, indicating that the decellularization process effectively preserves key protein compositions (Supplementary Figs. S4f and g).

In summary, the proteomic analysis of FDEM and ADEM revealed critical biochemical differences that likely drive the distinct cellular responses to these fetal and adult hydrogel systems. The retention of key structural and functional proteins, particularly in ADEM, underscores its potential to emulate the fibrochondrogenic native meniscus environment.

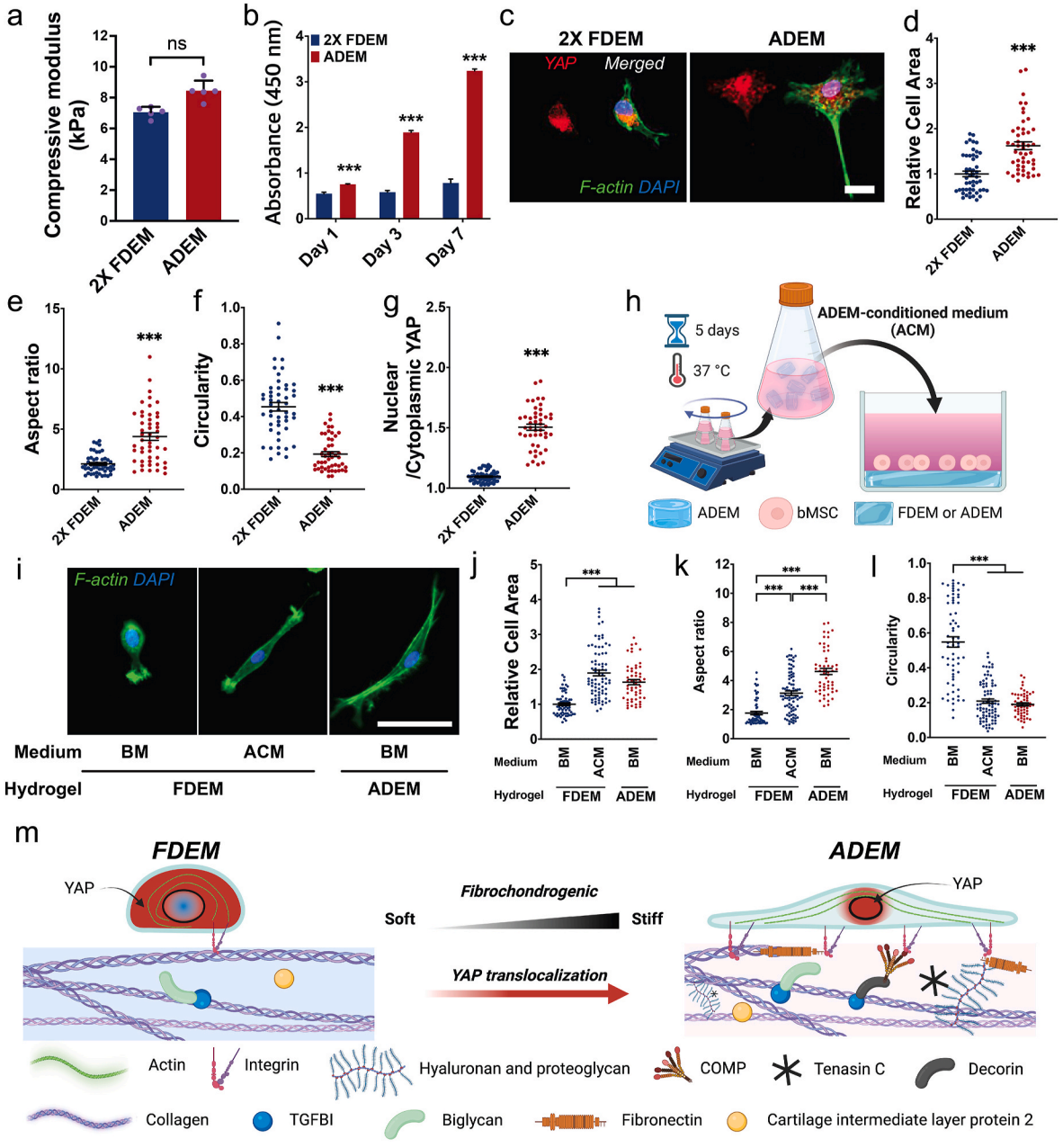

Fig. 4. Biochemical and Mechanical Effects of DEM Hydrogels. a) Compressive modulus of 2× FDEM and ADEM hydrogels (n = 5; ns: not significant). b) MSC proliferation on 2× FDEM and ADEM hydrogels at days 1, 3, and 7 (n = 5; ***: $p < 0.001$ vs. 2X FDEM). MSC morphology analysis after 3 days, including c) representative F-actin and YAP staining (Scale bar: 20 μm), d) relative cell area (n = 49), e) aspect ratio, f) circularity, and g) YAP nuclear localization (n = 46–57; ***$p < 0.001$ vs. 2× FDEM). h) Schematic showing experimental setup where media released from ADEM hydrogels is added to MSC cultures atop FDEM or ADEM hydrogels. Cell morphology under varied media and hydrogel conditions: i) Representative F-actin images (Scale bar: 50 μm). MSC morphology analysis, including j) relative cell area, k) aspect ratio, and l) circularity (n = 52–82; ***$p < 0.001$). m) Summary schematic illustrating the distinct biochemical and biomechanical microenvironments of the FDEM and ADEM hydrogels, highlighting that ADEM enhances fibrochondrogenic differentiation.

2.5. Decoupling effects of DEM hydrogel composition and stiffness on cellular response

Given that FDEM and ADEM hydrogels had distinct stiffnesses and biochemical compositions, we next sought to determine which of these factors drove the cellular response. To address this, we doubled the concentration in FDEM (2× FDEM) to achieve a compressive modulus comparable to that of ADEM hydrogels (Fig. 4a), standardizing the stiffness between the two systems. Interestingly, despite this adjustment, MSCs on 2× FDEM hydrogels still had a lower proliferation rate than those on ADEM (Fig. 4b). Moreover, cells on the 2× FDEM were smaller and more circular compared to their counterparts on ADEM hydrogels (Fig. 4c–f). This was further corroborated by significantly reduced YAP nuclear localization in MSCs on the 2× FDEM compared to ADEM hydrogels (Fig. 4g). These findings suggest that stiffness alone does not fully account for the varied cellular responses seen in FDEM and ADEM hydrogels, underscoring the importance of biochemical cues.

To further investigate the impact of biochemical composition, ADEM hydrogels were dissolved in basal growth media to prepare ADEM-conditioned media (ACM). MSCs were seeded on either FDEM or ADEM hydrogels and cultured with ACM or BM (as a control group, Fig. 4h). Interestingly, ACM culture prompted cells on FDEM hydrogels to enlarge and elongate, resembling the morphology of cells on ADEM hydrogels under BM conditions (Fig. 4i–l). Similar results were observed with MFCs cultured on tissue culture plates (TCP) (Supplementary Figs. S6a, c, and d) and ACM did not compromise cell viability (Supplementary Fig. S6b). Additionally, super-resolution H2B STORM imaging demonstrated that ACM culture reduced nanoscale chromatin condensation in MFC nuclei (Supplementary Figs. S6e and f), suggesting enhanced transcriptional activation in MFCs. Furthermore, DTAF and PSR staining confirmed that MFCs cultured in ACM produced more extracellular matrix and collagen than those in the control group (Supplementary Figs. S6g–i). These findings highlight the pivotal role of biochemical composition over mechanical stiffness in dictating cellular response to DEM hydrogels. The increased cell proliferation and morphological changes observed with ACM imply that specific biochemical factors inherent to ADEM are key drivers of these responses. The unique protein profiles revealed by proteomic analysis, particularly those associated with cell adhesion and ECM composition, may create a favorable microenvironment for cell adhesion, growth, and differentiation.

Taken together, this differential enhancement is crucial for meniscus tissue engineering, where regeneration of specific tissue types and functions is required. Notably, compared to FDEM, the fibrochondrogenic biochemical cues from ADEM alongside its stiffer biomechanical environment, significantly enhance cell attachment, proliferation, and YAP nuclear localization. These factors collectively foster an environment favorable to fibrochondrogenic differentiation and the formation of fibrous cartilage (Fig. 4m). These insights underscore the importance of biochemical signals in the design of tissue engineering scaffolds for meniscus repair and regeneration, highlighting the need for a tunable approach in scaffold design that integrates both mechanical and biochemical considerations to optimize regenerative outcomes.

2.6. Biochemically and mechanically tunable DEM-based hydrogels for zone-specific meniscus repair

Given the complexity of the meniscus, injectable materials tailored to specific meniscus zones are needed. Building from the zonal-specific cues provided by dECM of different ages, we next developed a stiffness-tunable DEM-based injectable hydrogel system. For this, we combined our DEM with methacrylated hyaluronic acid (MeHA), whose mechanics can be adjusted by controlling the degree of crosslinking (Fig. 5a) [40]. To first generate a ‘Soft’ MeHA and ‘Stiff’ MeHA component, the methacrylation level was set at 22 % and 100 %, respectively (Supplementary Figs. S7a and b). ‘Soft’ MeHA had a compressive modulus of 3.1 (±0.4) kPa while ‘Stiff’ MeHA was 16.2 (±2.3) kPa (Supplementary Fig. S7c). Next, the fetal and adult DEM and MeHA were combined in predetermined ratios (Fig. 5a). Fluorescence imaging (z-stack; z-axis distance: 200 μm) using FITC-labeled MeHA confirmed a homogeneous mixture of the two components (Supplementary Fig. S7e and Video 1). The resulting hydrogels exhibited a wide range of stiffness, from 4.4 kPa (FDEM) to 27.3 kPa (ADEM/Stiff MeHA) (Fig. 5b and Supplementary Fig. S7d and Table S1). By mixing ‘Soft’ and ‘Stiff’ at a 1:1 ratio, hydrogels with an intermediate stiffness were generated. Picrosirius red and Alcian blue staining confirmed that collagen content was preserved in the DEM and that proteoglycans were present due to the added MeHA (Supplementary Figs. S7f and g). These results demonstrated that, by modifying the methacrylation degree of HA, we could create DEM-based hydrogels with a broad range of stiffness values, to create tailored microenvironments for meniscus repair, potentially supporting the regeneration of specific tissue types and functions.

2.7. Cellular responses to tunable DEM-based hydrogel systems

Next, to determine how the presence of MeHA and the stiffness of tunable DEM-based hydrogels impacted cellular response, MSCs were cultured on the FDEM or ADEM hydrogels with or without the addition of ‘stiff’-MeHA. On these ‘stiff’ DEM-based hydrogel systems, incorporation of ‘stiff’ MeHA into fetal and adult hydrogels significantly increased cell area and YAP nuclear localization compared to FDEM or ADEM hydrogels (Fig. 5c–e).

Given that the FADEM hydrogel (a 1:1 mix of FDEM and ADEM) had mechanical and cellular characteristics intermediate between FDEM and ADEM hydrogels and contains both FDEM and ADEM proteins, we further examined cellular responses on FADEM-based stiffness-modulated MeHA hydrogels. When MSCs were cultured on FADEM-based MeHA hydrogels, cells on the ‘Soft’ hydrogels remained small and circular but elongated (Fig. 5f, g, Supplementary Figs. S7h, i) and increased YAP nuclear localization (Fig. 5f, h) with increased modulus. Notably, ‘Stiff’ FADEM-based hydrogel exhibited heightened COL1A2 expression, while the chondrogenic markers SOX9 and TGF increased in all MeHA-supplemented groups (Supplementary Fig. S7j). These data indicate that the introduction of MeHA to DEM elevated chondrogenic gene expression and that ‘stiff’ MeHA increased fibrochondrogenic gene expression in MSCs (Supplementary Fig. S7j).

To further understand changes in transcriptional profiles induced by the stiffness-tuned FADEM-based hydrogels, we performed whole-transcriptome analysis on two experimental conditions: ‘Soft’ and ‘Stiff’ FADEM-based hydrogels. Unsupervised clustering and PCA visualization (Supplementary Fig. S8a) showed that samples were clustered based on the stiffness of MeHA. After filtering for significant changes, genes were divided into two distinct clusters (Supplementary Fig. S8b). Applying thresholds (adjusted $p < 0.05$, $-2 >$ Fold change (FC), and FC > 2) identified 64 up-regulated and 414 down-regulated genes (Fig. 5i and Supplementary Table S2). Notably, in the ‘stiff’ FADEM-based microenvironment, meniscus ECM production, cell adhesion, cell migration, and cell development-related genes were upregulated (Fig. 5i). Further, heatmaps of differential gene expression confirmed that representative fibrogenic genes such as COL1A2 and COL3A1 were significantly expressed in the ‘stiff’ FADEM environment with upregulations of chondrogenic genes including COL2A1, ACAN, and TGFβ1 (Fig. 5j and Supplementary Fig. S8c). In contrast, genes related to chondrogenesis, including Cartilage oligomeric matrix protein (COMP) were more predominately expressed in ‘soft’ FADEM environment (Supplementary Fig. S8c). Moreover, the ‘stiff’ FADEM-based system enhanced gene expression related to cell adhesion, such as FN1 (Supplementary Fig. S8d). These findings confirm that the ‘soft’ FADEM hydrogels promote a chondrogenic phenotype, whereas ‘stiff’ FADEM drives cells towards a fibrocartilage phenotype.

GO analysis provided a more in-depth understanding of the

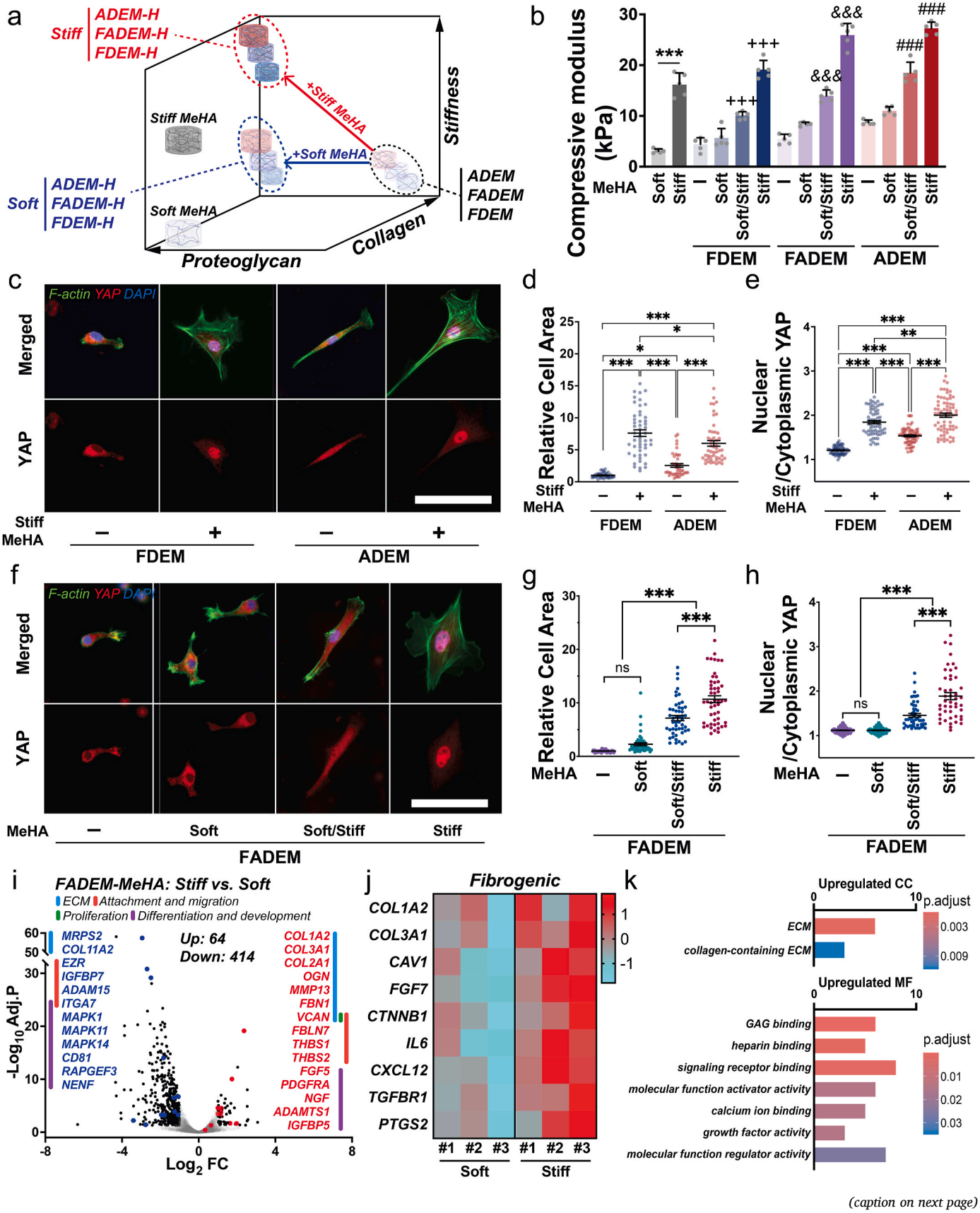

(caption on next page)

Fig. 5. Stiffness-tunable DEM-Based Hydrogels Direct MSC Phenotype. a) Illustration of strategies to develop tunable DEM-based hydrogel systems for zonal-specific meniscus tissue repair by including methacrylated hyaluronic acid (MeHA) of varied stiffness. b) Stiffness of mechanically modulated DEM-based hydrogels (n = 5; ***: p < 0.001, +++: p < 0.001 vs. FDEM, &&&: p < 0.001 vs. FADEM, ###: p < 0.001 vs. ADEM, p values for all comparison cases in Supplementary Table 2). MSC response to fetal and adult DEM-based hydrogels at day 3, including c) representative images on fetal and adult DEM-based hydrogel systems with or without the addition of 'stiff' MeHA (Green: F-actin, Red: YAP, and Blue: DAPI), d) relative cell area (n = 42–50; *p < 0.05, ***p < 0.001), e) YAP nuclear localization (n = 67–72; ***p < 0.001). MSC response to stiffness tunable FADEM-based hydrogels after 3 days, including f) representative images on FADEM hydrogels with or without 'soft', 'soft/stiff', or 'stiff' MeHA (Green: F-actin, Red: YAP, and Blue: DAPI), g) relative cell area (n = 50; *p < 0.05, ***p < 0.001), and h) YAP nuclear localization (n = 50; ***p < 0.001). Transcriptional analysis to compare MSCs on FADEM-Stiff MeHA (Treatment) vs. FADEM-Soft MeHA (Control) via RNA sequencing (n = 3/group), including i) Volcano plot, j) Z-score heat maps of fibrogenic gene expression, k) GO analysis of gene differentially expressed genes (CC: cellular components and MF: molecular functions).

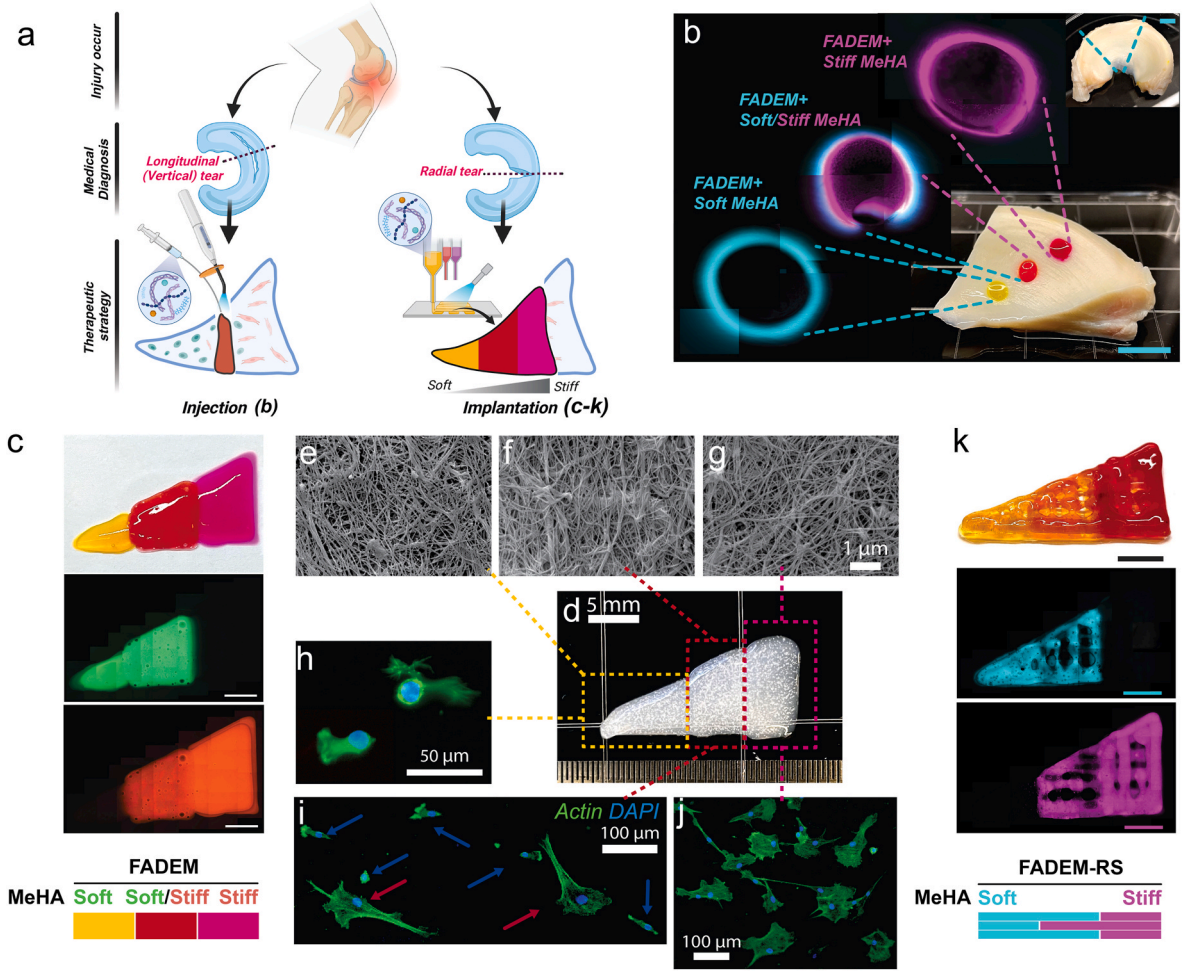

Fig. 6. Targeted Meniscus Repair Using Stiffness-Tunable DEM-Based Hydrogels. a) Illustration of the application of the system. *Injection method*: b) injected stiffness-modulated FADEM-based hydrogel in defects in different meniscus zones (scale bar: 5 mm). *Implantation method using 3D printed hybrid constructs*: c) images of a bioprinted stiffness-modulated FADEM-based hydrogel (yellow: printed 'soft' FADEM hydrogel for the inner meniscus zone, red: 'soft/stiff' FADEM hydrogel for the middle meniscus zone, purple: 'stiff' FADEM hydrogel for the outer meniscus zone, scale bar: 5 mm). (e–g) Representative FE-SEM images of fibrous structure of printed FADEM-based hydrogels. (h–j) F-actin staining of MSCs cultured on the zone-dependent printed FADEM-based hydrogels. (k) 3D printed lattices of zone-specific FADEM-based hydrogels with the addition of ruthenium/sodium persulfate (FADEM-RS, cyan: 'soft' FADEM, magenta: 'stiff' FADEM, scale bars: 5 mm).

biological processes involved: ECM-related cellular component genes were significantly upregulated in the 'stiff' FADEM group (Fig. 5k). Additionally, GO analysis revealed that genes related to the binding of major proteins including, glycosaminoglycan (GAG) and heparin, and cellular activities were significantly upregulated in the 'stiff' FADEM hydrogels (Fig. 5k). Those data indicate that the 'stiff' FADEM microenvironment appears to accelerate cellular and ECM protein production and maturation compared to the 'soft' FADEM microenvironment. Taken together, these findings demonstrate that by fine-tuning the stiffness of FADEM-based hydrogels, we can create tailored microenvironments that influence MSC behavior and phenotype.

Finally, to further evaluate the biocompatibility and integration of tunable FADEM-based hydrogel *in vivo*, bovine meniscus explants were prepared by filling FADEM-based hydrogels (Supplementary Fig. S9a) and implanted subcutaneously into mice (Supplementary Fig. S9b). Three weeks post-implantation, the implants were fully integrated with the host tissue (Supplementary Fig. S9c). No adverse tissue reaction was observed in any of the groups and histological results were consistent across all groups (Supplementary Figs. S9d-e). In the 'soft' FADEM group, a considerable number of cells infiltrated into the hydrogel, while in the 'stiff' FADEM group, a small number of cells were observed migrating at the junction of the scaffold and hydrogel in the central region, forming a thin layer. This phenomenon could be attributed to the differences in the stiffness and degradability of the hydrogels,

corroborating the cell infiltration and migration observed in animal experiments.

2.8. Application of stiffness-tunable DEM-based hydrogels for precision meniscus repair

The tunable properties of the stiffness-tunable DEM-based hydrogel system offers a promising avenue for the treatment of diverse meniscus tears by virtue of their tailored the biochemical and biomechanical properties. For example, in the case of either small or longitudinal (vertical) tears within a specific region, a single injection could prove effective, where hydrogels with varying degrees of stiffness — ranging from 'soft', to 'soft/stiff', to 'stiff'— could be strategically administered into the meniscus tissue's inner, intermediate, and outer zones, respectively (Fig. 6a and b). Alternatively, for more complex injuries, such as radial tears that begin in the inner meniscus and extend to the peripheral edge, the stiffness tunable DEM-based material system could be coupled with advanced fabrication techniques such as 3D bioprinting (Fig. 6a and c-k). Employing our stiffness-tunable FADEM-based materials ('soft', 'soft/stiff', and 'stiff' FADEM), we crafted a hybrid hydrogel containing biomaterial and mechanical gradients. These gradients were produced using a multi-head 3D bioprinting system to mimic the zonal properties of the tissue (Fig. 6c). FE-SEM analysis verified the retention of fibrous structures after printing (Fig. 6e–g). Additionally, distinct zonal-dependent cell morphologies were observed when MSCs were cultured on the 3D printed construct, with smaller and rounder cells on the 'soft' hydrogel region (Fig. 6h) and larger and elongated cells on the 'stiff' region (Fig. 6j), with a mix of cell populations in the 'soft/stiff' region (Fig. 6i). This highlights the capability of the system to effectively emulate the cell morphology of native meniscus tissue by adjusting hydrogel properties.

To further improve the printability of DEM-based materials and the integrity of the printed structures, we introduced a rapid curing reaction with the addition of ruthenium (Ru)/sodium persulfate (SPS) (Fig. 6k). The Ru/SPS visible photoredox system interacts with tyrosine proteins prevalent in DEM, encouraging dityrosine bond formation for rapid cross-linking [41]. Through a triple crosslinking process utilizing heat, UV, and visible light during 3D bioprinting, we created 3D-printed hybrid structures with interconnected pores using 'soft' and 'stiff' FADEM-based hydrogels (Fig. 6k). This improved structural fidelity not only benefits tissue engineering but also enhances the material's physical and biochemical characteristics. The introduction of pores may support proper cell infiltration and differentiation based on the meniscus zone, potentially fostering the development of heterogeneous tissue structures that more closely resemble the native meniscus.

3. Discussion

Current meniscus tissue engineering strategies are limited by their inability to replicate the complex zonal-dependent properties of meniscal tissue [1]. For instance, currently used biomaterials based on collagen and synthetic scaffolds do not mimic these zonal characteristics, leading to suboptimal healing and functional outcomes [2]. Similarly, traditional surgical interventions like suturing and arthroscopic partial meniscectomy (APM) fail to address the meniscus's biochemical and structural heterogeneity in the meniscus tissue [3]. To address these limitations, we introduced a novel approach for meniscus repair through the development of a tunable DEM-based hydrogel system, designed to approximate the zonal heterogeneity of the native meniscus tissue. The goal of this study was to engineer a biomimetic material capable of emulating the distinct biochemical and mechanical profiles of the meniscus zones, thereby enhancing cell compatibility, guiding accurate zone-dependent cell differentiation, and improving healing outcomes.

In this study, we successfully synthesized fetal and adult hydrogels (FDEM and ADEM) that distinctly influenced cell behavior based on the donor tissue's age used to prepare the DEM. The fetal and adult meniscus DEMs were derived from powdered and lyophilized tissues, which, while effective in retaining essential biochemical properties confirmed by mass spectrometry, may not fully replicate the native meniscus's complex collagen fibrous-fibrillar-bundle structure. Future studies need to focus on refining tissue processing methods to better preserve or replicate the hierarchical collagen architecture critical to meniscus function. Furthermore, additional investigations into protein expression changes in cells in response to age-specific hydrogel systems are needed to deepen our understanding of the underlying cellular and molecular mechanisms that drive these distinct responses.

Proteomic analyses corroborated these findings, revealing a higher abundance of cell adhesion and fibrochondrogenic proteins in ADEM. Notably, the exclusive presence of fibronectin in ADEM, a pivotal protein for cell adhesion and proliferation, alongside its interaction with structural proteins like collagen, underscores the unique properties of the ADEM system in promoting cellular attachment and proliferation [42]. Additionally, blending different DEM types (i.e., FADEM) offers the opportunity to generate a spectrum of biochemical and mechanical stimuli. Moreover, unlike hydrogels requiring chemical additives (e.g., TGF-β3 or CTGF), our DEM hydrogels retain their age-specific properties post-decellularization, potentially offering a more advanced replication of the native tissue milieu and delivering biomechanical and biochemical signals that naturally modulate cell behavior. Indeed, our explant assays confirmed that DEM hydrogels can recruit cells from the surrounding native tissue. Collectively, these findings demonstrate the unique capacity of DEM hydrogels to emulate the native tissue environment and provide tailored biomechanical and biochemical cues to direct cellular responses and, consequently, the success of regenerative therapies.

Despite their inherent advantages, DEM hydrogels alone may not fully capture the specific mechanical properties essential for recapitulating the region-specific properties of the meniscus. To overcome this, we combined the fetal and adult DEM with MeHA, a biomaterial known for its tunable mechanical properties [43]. This combination harnesses the biological benefits of DEM while providing further mechanical tunability via MeHA crosslinking, allowing for a more refined calibration of hydrogel stiffness. In addition, the decellularization process typically leads to a reduction in GAG content [44], which is vital for biomechanical integrity in the meniscus. The addition of MeHA may compensate for this loss, replenishing hydration and mechanical attributes of the hydrogel. The MeHA-modified DEM hydrogels potentially create an optimized mechanical and biochemical milieu that promotes targeted cell proliferation and differentiation, mimicking the unique characteristics of various regions within the meniscus. Indeed, DEM-based 'stiff' MeHA hydrogels directed increased cell attachment and YAP nuclear localization, with FDEM-based 'stiff' MeHA hydrogels surpassing the effects observed with ADEM on its own. These findings suggest that the DEM-MeHA hydrogel system not only aids in restoring mechanical and biochemical composition but also regulates cellular behavior. While the study primarily focused on the compressive properties, given the hydrogel's potential for injection, future studies will need to consider its tensile properties. Furthermore, although the stiffness of the tunable hydrogel does not fully replicate the mechanical properties of native meniscus tissue, the goal of this system is not to entirely replace the meniscus. Instead, it is intended for injection into partial meniscal injuries, where it can support the healing process by creating a dynamic environment that fosters tissue regeneration. Thus, the DEM-MeHA hydrogels present a promising, customizable solution for meniscus repair.

In addition to its role in mechanical tuning, MeHA also improves the injectability of the DEM-based hydrogel, a critical feature for minimally invasive meniscus repair techniques [45]. This enhanced injectability could enable simpler biomaterial delivery and better *in situ* integration. Active cell recruitment support of the DEM-MeHA hydrogel system observed through animal experiments effectively supports the induction of cell differentiation by providing cells with a pre-designed

microenvironment. MeHA also augments the bioprintability of the hydrogel, which is advantageous for 3D bioprinting applications, crucial for fabricating heterogeneous and anatomically precise scaffolds. The injectable and 3D-printable nature of the DEM-MeHA composite hydrogel broadens its clinical applicability, facilitating minimally invasive delivery and personalized scaffold production, thus improving the practicality of meniscus repair interventions. This study comprehensively evaluated the DEM-based hydrogel system through *in vitro*, *ex vivo*, and *in vivo* tests using a small animal model. While the subcutaneous implantation model provided valuable preliminary insights into the hydrogel's biocompatibility, degradation, and cellular infiltration, this model does not replicate the complex mechanical microenvironment of the knee joint, where the meniscus resides. Thus, further assessment in a more clinically relevant large animal meniscus injury model is still needed to validate its effectiveness for meniscus tissue repair following hydrogel injection under physiologically relevant mechanical loading conditions.

Additionally, while the current approach focuses on an acellular hydrogel system to enhance endogenous cell recruitment and promote tissue repair, future research could explore the synergistic effects of integrating cell-embedded hydrogels or soluble growth factors with injectable delivery and cell-printing technologies. This approach offers a promising avenue for enhancing regenerative outcomes. Furthermore, while bovine ECM was used in this study as a proof of concept due to its consistent availability, future studies will prioritize the use of human-derived ECM to better align with clinical applications and minimize potential species-specific differences in cellular responses. Human meniscus ECM is expected to more closely reflect the physiological and mechanical properties necessary for successful tissue regeneration in clinical settings. Therefore, future studies will explore human-derived ECM to investigate ways to bridge the gap toward clinical application. In addition, this study mainly utilizes juvenile bovine cell donors to provide valuable insights into the regenerative potential of our hydrogel system. However, clinical translation necessitates evaluating its performance using adult tissues and cells. Therefore, future studies should incorporate adult meniscus cells and tissues into experimental models to more effectively assess how the hydrogel supports repair and regeneration in clinically relevant contexts. This approach will allow for a more comprehensive evaluation of the hydrogel's potential in meniscus repair and regeneration.

Taken together, our tunable DEM-based hydrogel system advances the field by providing a flexible approach to craft tailored microenvironments for tissue regeneration. The precise control over hydrogel stiffness and the ability to modulate cellular response based on both composition and stiffness enables targeted regenerative therapies that may improve outcomes for meniscus repair and beyond. This study represents a significant advance in tissue engineering, offering a promising platform for developing targeted regenerative therapies that could lead to improved clinical outcomes and a deeper understanding of mechanobiological influences in musculoskeletal repair. Furthermore, the adaptability of our hydrogel systems positions them as a formidable tool for a broad spectrum of biomedical applications, ranging from *in vitro* disease modeling to *in vivo* regenerative treatments.

4. Materials and methods

4.1. Preparation of fetal and adult meniscus decellularized ECM (DEM) powder

Bovine fetal (3rd trimester) and adult (~30-month-old) menisci for decellularization were purchased (Animal Technologies, Inc., USA) and meniscus tissues were decellularized following a previously reported protocol with minor adjustments [41,46,47]. Briefly, the menisci were chopped into 2 mm^3 cubes and stirred in deionized water for 4 h to remove blood. Next, the tissues were decellularized in a solution of 0.3 % (w/v) sodium dodecyl sulfate (Invitrogen, USA) in phosphate buffered saline (PBS; Growcells, USA) for 24 h, followed by treatment with 3 % (v/v) Triton-X100 (Sigma Aldrich; USA) in PBS for 24 h, and 7.5 U/ml Deoxyribonuclease (Sigma Aldrich, USA) in PBS for 24 h. To sterilize the treated tissues, tissues were rinsed with 4 % ethyl alcohol for 4 h. Residual chemicals were removed by rinsing the treated tissues with PBS between each treatment step. After lyophilization, the tissues were crushed into powder using a liquid nitrogen cryomill (14 cycle per second) to yield fetal and adult meniscus dECM powders.

4.2. Fabrication of fetal and adult meniscus DEM hydrogels

To prepare DEM-based hydrogels, the fabricated fetal and adult meniscus DEM powders were each digested in a 0.5 M acetic acid solution (Sigma-Aldrich, USA) with pepsin (Sigma-Aldrich, USA) at room temperature for 72 h. After filtration through a 40 μm pore mesh, the digested solution was neutralized using a 10 N NaOH solution (Sigma-Aldrich, USA). The DEM pre-gel was prepared by adding 10 × PBS and sterilized water into the neutralized DEM solution. Fetal DEM (FDEM) and adult DEM (ADEM) hydrogels were fabricated by cross-linking the prepared pre-gel at 37 $^{\circ}C$ for 30 min. To create a composite group comprised of both the fetal and adult DEM, fetal and adult DEM (FADEM), the prepared FDEM and ADEM pre-gels were mixed in a 1:1 ratio. A 1.5 wt% concentration of FADEM was used for experiments [44]. To examine fibrous structures in DEM, the fabricated DEM gels were dried at room temperature, coated with platinum using a sputter coater, and imaged using a FEI Quanta FEG 250 scanning electron microscope (SEM; ThermoFisher, USA) at magnification of 5000×. The distribution of fiber diameters was analyzed using ImageJ (National Institutes of Health, USA).

4.3. Protein identification by mass spectrometry (LC-MS/MS)

To analysis protein components in the fabricated Fetal and Adult DEM, proteomic analysis was performed. To prepare samples, the fetal and adult bovine menisci with four different donors were decellularized in the same protocol as prementioned. The DEM powder was fabricated through the lyophilization and cryomill procedures and used for the proteomic analysis. A mass spectrometry (LC-MS/MS) was performed as described in Supplementary information. Only proteins detected in two or more of the four different donors were processed for analysis. Differential level of proteins was identified with criteria of p-value <0.05 and absolute $\log_2$ (Fold change) > 1.0 for volcano plot. Gene symbols corresponding to the identified proteins were input into the STRING web tool (version 10.0, http://string.embl.de, String Consortium 2020) to obtain data on protein-protein networks [48]. The acquired data were then imported into Cytoscape (Version 3.10.1) for visualization and annotation [49]. Gene ontology (GO) analysis was conducted using the STRING web tool, which identified biological process (BP), cellular component (CC), and molecular function (MF) terms with a corrected p-value <0.05.

4.4. Fabrication and characterization of stiffness tunable DEM-based MeHA hydrogels

Sodium hyaluronic acid (HA; Lifecore Biomedical, USA) was methacrylated as previously described [43,50,51]. Briefly, methacrylate HA (MeHA) was obtained by methacrylate esterification with the hydroxyl group of the 68 kDa sodium HA. The degree of the methacrylation was controlled by adjusting the amount of methacrylic anhydride (Sigma Aldrich, USA), with target methacrylation degrees of ~30 % ('soft') and 100 % ('stiff'). After dialysis at room temperature, stiffness-modulated MeHA macromers were isolated by freezing and lyophilizing. Lyophilized polymers were dissolved in deuterium oxide (Sigma Aldrich, USA) at a concentration of 10 mg/mL and analyzed using ^{1}H NMR (Bruker NEO400, USA) to determine the degree of modification [52].

To fabricate DEM-based MeHA hydrogels with different stiffness,

Fetal and adult DEM and the stiffness-tuned MeHA system (soft or stiff) was blended to a final concentration of 1.5 wt% and 1.0 wt% final concentrations, respectively. In another group, soft and stiff MeHA were mixed at a 1:1 ratio. Thiolated fluorescein peptide (GenScript, USA, 2.0–2.5 %) was incorporated during crosslinking to observe the homogeneous blending of the FITC-Soft/Stiff MeHA and DEM. The thiol groups from the fluorescein peptide and the methacrylate groups from the MeHA macromers were conjugated via Michael addition reactions [53]. After dialysis, the fluorescein peptide-conjugated MeHA macromers were isolated through freezing and lyophilization. To assess the homogeneity of these macromers, a confocal microscope (TCS SP8 STED, Leica, Germany) was employed. The macromers were scanned over an area of 1.5 mm × 1.5 mm to a depth of 200 μm (Z stack; 10× magnification) to evaluate their distribution and uniformity.

A custom mechanical testing device was used to evaluate compressive moduli of the fabricated hydrogels [54]. For this, the hydrogel samples were prepared in cylindrical molds measuring 5 mm diameter and 2 mm thickness. Samples were equilibrated in creep under a static load of 0.1 g for 5 min. After creep, samples were subjected to 50 % strain applied at 0.5 %/s. The compressive modulus was determined from the stress (minus tare stress) normalized to the applied strain in the linear region.

4.5. Cell isolation and in vitro culture

Cell isolation for in-vitro testing was performed as previously reported [55,56]. Briefly, juvenile bovine knee joints (2–3 months old; Research 87, USA) were acquired. Bone marrow derived mesenchymal stem cells (MSCs) were isolated from the femur and tibia, and meniscal fibrochondrocytes (MFCs) were isolated from the meniscus. Cells were cultured in basal growth media [BM; Dulbecco's modified Eagle's medium (DMEM; Gibco, USA) supplemented with 10 % fetal bovine serum (R&D systems, USA) and 1 % Penicillin Streptomycin (Gibco, USA)]. Cells at passage 2 were used for in-vitro experiments. To prepare ADEM-conditioned media (ACM), ADEM was added to fresh BM and incubated at 37 °C with shaking for 5 days. Concurrently, fresh BM was also incubated under the same conditions with ACM, serving as the control group (Ctrl). After filtration through a 40 μm pore mesh, the ACM with a 3.3 % v/v concentration was used for the dissolution test *in vitro*, having confirmed its low cytotoxicity via a Live/Dead assay. The DEM system was coated onto a 24-well tissue culture plate and cross-linked in a CO2 incubator for 30 min. For the DEM-based MeHA system, an additional crosslinking step was performed by exposing it to 15–20 mW/cm^2 UV light (Omnicure S2000-XLA, Lumen Dynamics, Canada) for 30 min. Following crosslinking, cells were seeded on the surface of the coated DEM or DEM-based MeHA systems and cultured in either BM or ACM.

4.6. Metabolic and cytotoxicity assays

The DEM-based MeHA hydrogel was added to a 24-well plate to completely cover the bottom surface. Cells were then seeded at a density of 1×10^5 cells per well (n = 5/group). Proliferation of seeded cells was determined using a Cell Counting Kit-8 assay (CCK-8; Dojindo, Japan). After 1, 3, and 7 days, medium containing 10 % CCK-8 agent was added to each well and incubated at 37 °*C* for 4 h. The absorbance of each well was measured at 450 nm using a Synergy H1 microplate reader (BioTek, USA). Cell viability was assessed using the Live/dead kit (Invitrogen, USA). Live cells were stained by Calcein AM and dead cells were stained by Ethidium homodimer-1. After imaging, quantification was performed in ImageJ (n = 5).

4.7. Analysis of cell morphology and YAP nuclear localization

Immunofluorescence staining was performed to measure cell morphology and YAP (Yes-associated protein) in cells cultured on hydrogels. Cells were fixed at day 3 with 4 % paraformaldehyde (PFA). To examine cell morphology, cells were permeabilized with Triton X-100 and stained with Phalloidin-Alexa488 (Invitrogen, USA) to visualize actin. Nuclei were labeled with ProLong™ Gold antifade reagent with DAPI (Invitrogen, USA). For YAP staining, cells were incubated with anti-YAP antibody (Santa Cruz Biotechnology, USA) followed by Alexa Fluor546-goat anti-mouse IgG (Life technologies, USA). Images were obtained using a widefield fluorescent microscope (Leica, Germany). Cell morphology and YAP nuclear localization were analyzed with ImageJ.

4.8. Gene expression analysis

Messenger RNA was extracted from the MSCs or MFCs cultured on hydrogels using the TRIzol/chloroform method [54]. The concentration of the total RNA was determined using a spectrophotometer (Nano-drop Technologies, USA) [50]. Subsequently, cDNA was synthesized using PhotoScript II First-Strand cDNA Synthesis Kit (New England BioLabs, USA). Reverse transcription-polymerase chain reaction (RT-PCR) was performed on a QuantStudio 6 Pro (Applied Biosystems, USA) with Fast SYBR Green Master Mix (Applied Biosystems, USA). The expression of collagen type I alpha 2 chain (COL1A2), Collagen Type-2 (COL2), Collagen Type-3 (COL3), Connective tissue growth factor (CTGF), Aggrecan (ACAN), SRY-box Transcription Factor 9 (SOX9), and Transforming growth factor (TGF) were determined. Expression levels were normalized to the house-keeping gene Glyceraldehyde 3-phosphate dehydrogenase (GAPDH). Primer sequences are provided in Table 1.

4.9. RNA sequencing

RNA sequencing was carried out with the MSCs cultured on FADEM-based 'Soft', 'Stiff' hydrogels. Each type of hydrogel was coated on the bottom surface of 24-well tissue culture plates and cross-linked under UV and 37 °C. Passage 2 (P.2) cells were seeded in the 24-well tissue culture dishes at a density of 1×10^5 cells per well. The cells were cultured in basal growth media for 7 days. Total RNA was extracted from the cells on the hydrogel surface using the TRIzol/chloroform method [54]. RNA-Seq library preparation (including rRNA depletion) and sequencing (150 bp paired-end) were performed at Genewiz (South Plainfield, New Jersey). Sequence reads were processed using Trimmomatic v.0.36 to trim potential adapter sequences and low-quality nucleotides. The processed reads were aligned to the *Bos taurus* reference genome (available on Ensembl) with the STAR aligner v.2.5.2b. Unique gene hit counts were determined using featureCounts from the Subread package v.1.5.2. Differential expression analysis between the experimental conditions, FADEM-based Soft MeHA and FADEM-based Stiff MeHA, was conducted using the DESeq2 package in R. Global

Table 1
Primer sequence for quantitative real-time PCR analysis.

Gene		Sequence
Bovine-COL1A2	Forward	AATTCCAAGGCCAAGAAGCATG
	Reverse	GGTAGCCATTTCCTTGGTGGTT
Bovine-COL2	Forward	GTGTCAGGGCCAGGATGTC
	Reverse	GCAGAGGACAGTCCCAGTGT
Bovine-COL3	Forward	CTGACATTTAGACATGATGAG
	Reverse	ACTGACCGAGATGGGAGCAT
Bovine-CTGF	Forward	CGTGTGCACCGCTAAAGATG
	Reverse	GGAAAGACTCTCCGCTCTGG
Bovine-ACAN	Forward	CCTGAACGACAAGACCATCGA
	Reverse	TGGCAAAGAAGTTGTCAGGCT
Bovine-SOX9	Forward	TGAAGAAGGAGAGCGAGGAG
	Reverse	GTCCAGTCGTAGCCCTTGAG
Bovine-TGF	Forward	CACGTGGAGCTGTACCAGAA
	Reverse	ACGTCAAAGGACAGCCACTC
Bovine-GAPDH	Forward	ATCAAGAAGGTGGTGAAGCAGG
	Reverse	TGAGTGTCGCTGTTGAAGTCG

transcriptional changes across the groups were visualized with GraphPad Prism. The DESeq2 Likelihood Ratio Test (LRT) was employed to assess differential expression between the contrasts of interest, with a stringent significance threshold of $p < 0.05$ to ensure a high level of confidence in rejecting the null hypothesis. Differentially expressed genes (DEGs) were identified using the DESeq2 package with criteria of Benjamini-Hochberg adjusted p-value <0.05 and absolute log2 (fold change) > 1.0. The R pheatmap package was utilized to illustrate the expression patterns, clusters, and distribution of significant genes from the LRT analysis. To achieve a deeper insight into the functional profiling of genes significant in the LRT analysis, a gene enrichment analysis was conducted to identify highly enriched biological processes. This analysis was performed using the g function on the gProfiler web server (https://biit.cs.ut.ee/gprofiler/gost). The significance threshold was set using the Benjamini-Hochberg FDR (false discovery rate), with significant Gene Ontology (GO) terms defined by an adjusted p-value of <0.05. For visualization, the significant GO terms were created using the ggplot2 package in R.

4.10. Ex-vivo evaluation of fetal and adult meniscus DEM hydrogels in meniscus defects

Whole menisci were dissected from fresh juvenile bovine knees, and radial incisions were made. Using biopsy punches, a 3 mm diameter hole was created in the avascular zone of each cross-section, and the DEM-based hydrogel was injected into the holes [57]. (Fig. 2i). The defect group, serving as a control, was left unfilled. The tissues were cultured for 3 weeks in basal growth media. For histological analysis, tissues were fixed in 4 % paraformaldehyde, embedded in Cryoprep frozen section embedding medium, and sectioned at a thickness of 8 μm. Hematoxylin and eosin (H&E) staining was carried out to evaluate the DEM matrix preservation and cell infiltration during the culture period. The number of nuclei present in the H&E images was counted using ImageJ. Picrosirius red (PSR) staining was performed to visualize collagen. Additional tissues with injected DEM gel were fixed in 4 % paraformaldehyde, infiltrated with Citrisolv, embedded in paraffin, and sectioned at 3 weeks. H&E staining was conducted to confirm cell recruitment into the injected DEM gel. The nuclear area on the H&E images was measured in ImageJ, and the PSR staining was performed to visualize collagen.

4.11. Extrusion-based 3D printing

FADEM-based hydrogels were printed using a BIO X 3D bioprinter (Cellink, Sweden). To prepare the FADEM-based MeHA hydrogel, FDEM and ADEM hydrogels were neutralized with 10 M NaOH. A blend of FADEM blended with 'soft,' 'soft/stiff,' or 'stiff' MeHA was created, and the final concentration was designed to be 1.5 wt% FADEM-1.0 wt% MeHA. Then, they were loaded into syringes and stored at 4 °C. Extrusion was performed using 22 G nozzles with pneumatic pressures ranging from 10 to 30 kPa. The formed hydrogels were exposed to 18–24 mW/cm^2 UV light (365 nm wavelength) during the extrusion process. To distinguish the printed materials, Rhodamine B and Fluorescein disodium salt (AquaPhoenix Scientific, USA) were added before the 3D printing process. To enhance the printability of the DEM-based hydrogel systems, Ruthenium/sodium persulfate (RS, $1/10 \times 10^{-3}$ M R/S) was added to the DEM-MeHA hydrogels. The same printing conditions were maintained, with visible light (>405–450 nm wavelength) at 10–30 mW/cm^2 applied simultaneously during material extrusion [41].

4.12. Statistical analysis

All data are presented as the mean ± standard deviation. Statistical analysis was performed using one-way analysis of variance (ANOVA) with Tukey's *post hoc* testing with a 95 % confidence interval via GraphPad Prism version 9 software (San Diego, USA). A p-value less than 0.05 was considered statistically significant.

CRediT authorship contribution statement

Se-Hwan Lee: Writing – review & editing, Writing – original draft, Visualization, Validation, Supervision, Software, Project administration, Methodology, Investigation, Funding acquisition, Formal analysis, Data curation, Conceptualization. **Zizhao Li:** Writing – review & editing, Validation, Methodology, Formal analysis, Data curation, Conceptualization. **Ellen Y. Zhang:** Writing – review & editing, Validation, Software, Methodology, Formal analysis, Conceptualization. **Dong Hwa Kim:** Writing – review & editing, Validation, Methodology, Formal analysis, Conceptualization. **Ziqi Huang:** Writing – review & editing, Formal analysis, Data curation, Conceptualization. **Yuna Heo:** Methodology, Data curation. **Sang Jin Lee:** Writing – review & editing, Visualization, Validation, Formal analysis, Data curation, Conceptualization. **Hyun-Wook Kang:** Writing – review & editing, Supervision, Formal analysis, Conceptualization. **Jason A. Burdick:** Writing – review & editing, Formal analysis, Conceptualization. **Robert L. Mauck:** Writing – review & editing, Supervision, Funding acquisition, Formal analysis, Conceptualization. **Su Chin Heo:** Writing – review & editing, Writing – original draft, Visualization, Validation, Supervision, Resources, Project administration, Methodology, Funding acquisition, Formal analysis, Conceptualization.

Ethics approval and consent to participate

The animal study was approved by the Committee of the Use of Live Animals in Teaching and Research (CULATR) at the University of Hong Kong (Animal research Protocol No. 22–268).

Declaration of competing interests

The authors declare no competing interests.

Acknowledgments

This research was supported by the National Institutes of Health (K01 AR07787, R21 R077700, P30 AR069619, R01 AR056624, R01 HL163168), National Science Foundation (CMMI 1548571), and Department of Veterans Affairs (CReATE Motion Center, I50 RX004845) in the United States. This research was supported by the Korea Health Technology R&D Project through the Korea Health Industry Development Institute (KHIDI) funded by the Ministry of Health and Welfare (HI19C1095) and National R&D Program through the National Research Foundation of Korea (NRF) funded by Ministry of Science and ICT (RS-2024-00405574) in the Republic of Korea.

Appendix A. Supplementary data

Supplementary data to this article can be found online at https://doi.org/10.1016/j.bioactmat.2025.02.013.

References

[1] M. Sweigart, C. Zhu, D. Burt, P. DeHoll, C. Agrawal, T. Clanton, K.A. Athanasiou, Intraspecies and interspecies comparison of the compressive properties of the medial meniscus, Ann. Biomed. Eng. 32 (2004) 1569–1579.
[2] C.A. Murphy, G.M. Cunniffe, A.K. Garg, M.N. Collins, Regional dependency of bovine meniscus biomechanics on the internal structure and glycosaminoglycan content, J. Mech. Behav. Biomed. Mater. 94 (2019) 186–192.
[3] T.K. Tsinman, X. Jiang, L. Han, E. Koyama, R.L. Mauck, N.A. Dyment, Intrinsic and growth-mediated cell and matrix specialization during murine meniscus tissue assembly, FASEB J. 35 (8) (2021) e21779 official publication of the Federation of American Societies for Experimental Biology.
[4] A. Abbadessa, J. Crecente-Campo, M.J. Alonso, Engineering anisotropic meniscus: zonal functionality and spatiotemporal drug delivery, Tissue Eng. B Rev. 27 (2) (2021) 133–154.

[5] J. Twomey-Kozak, C.T. Jayasuriya, Meniscus repair and regeneration: a systematic review from a basic and translational science perspective, Clin, Sports Med. 39 (1) (2020) 125–163.

[6] F. Porzucek, M. Mankowska, J.A. Semba, P. Cywoniuk, A. Augustyniak, A. M. Mleczko, A.M. Teixeira, P. Martins, A.A. Mieloch, J.D. Rybka, Development of a porcine decellularized extracellular matrix (DECM) bioink for 3D bioprinting of meniscus tissue engineering: formulation, characterisation and biological evaluation, Virtual Phys. Prototyp. 19 (1) (2024) e2359620.

[7] J. Pak, J.H. Lee, K.S. Park, J.H. Jeon, S.H. Lee, Potential use of mesenchymal stem cells in human meniscal repair: current insights, Open Access J. Sports Med. (2017) 33–38.

[8] M.M. Higashioka, J.A. Chen, J.C. Hu, K.A. Athanasiou, Building an anisotropic meniscus with zonal variations, Tissue Eng. 20 (1–2) (2014) 294–302.

[9] M.I. González-Duque, A.M. Flórez, M.A. Torres, M.R. Fontanilla, Composite zonal scaffolds of collagen I/II for meniscus regeneration, ACS Biomater. Sci. Eng. 10 (4) (2024) 2426–2441.

[10] H.-W. Yun, B.R. Song, D.I. Shin, X.Y. Yin, M.-D. Truong, S. Noh, Y.J. Jin, H. J. Kwon, B.-H. Min, Fabrication of decellularized meniscus extracellular matrix according to inner cartilaginous, middle transitional, and outer fibrous zones result in zone-specific protein expression useful for precise replication of meniscus zones, Mater. Sci. Eng. C 128 (2021) 112312.

[11] P.X. Bradley, K.N. Thomas, A.L. Kratzer, A.C. Robinson, J.R. Wittstein, L. E. DeFrate, A.L. McNulty, The interplay of biomechanical and biological changes following meniscus injury, Curr. Rheumatol. Rep. 25 (2) (2023) 35–46.

[12] S. Bansal, E.R. Floyd, M. A Kowalski, E. Aikman, P. Elrod, K. Burkey, J. Chahla, R. F. LaPrade, S.A. Maher, J.L. Robinson, Meniscal repair: the current state and recent advances in augmentation, J. Orthop. Res. 39 (7) (2021) 1368–1382.

[13] A. Avila, K. Vasavada, D.S. Shankar, M. Petrera, L.M. Jazrawi, E.J. Strauss, Current controversies in arthroscopic partial meniscectomy, Curr. Rev. Musculoskelet. Med. 15 (5) (2022) 336–343.

[14] Y. Hashimoto, K. Nishino, K. Orita, S. Yamasaki, Y. Nishida, T. Kinoshita, H. Nakamura, Biochemical characteristics and clinical result of bone marrow–derived fibrin clot for repair of isolated meniscal injury in the avascular zone, Arthrosc. J. Arthrosc. Relat. Surg. 38 (2) (2022) 441–449.

[15] J.M. Woodmass, R.F. LaPrade, N.A. Sgaglione, N. Nakamura, A.J. Krych, Meniscal repair: reconsidering indications, techniques, and biologic augmentation, JBJS 99 (14) (2017) 1222–1231.

[16] M. Keagle, V. Gallicchio, Stem cell administration to repair torn menisci, Stem Cells Regen Med 7 (1) (2023) 1–29.

[17] Z. Li, W. Yan, F. Zhao, H. Wang, J. Cheng, X. Duan, X. Fu, J. Zhang, X. Hu, Y. Ao, Regional specific tunable meniscus decellularized extracellular matrix (MdECM) reinforced bioink promotes anistropic meniscus regeneration, Chem. Eng. J. 473 (2023) 145209.

[18] A. Tsujii, N. Nakamura, S. Horibe, Age-related changes in the knee meniscus, Knee 24 (6) (2017) 1262–1270.

[19] S. Bansal, J.M. Peloquin, N.M. Keah, O.C. O'Reilly, D.M. Elliott, R.L. Mauck, M. H. Zgonis, Structure, function, and defect tolerance with maturation of the radial tie fiber network in the knee meniscus, J. Orthop. Res. 38 (12) (2020) 2709–2720.

[20] L.C. Ionescu, G.C. Lee, G.H. Garcia, T.L. Zachry, R.P. Shah, B.J. Sennett, R. L. Mauck, Maturation state-dependent alterations in meniscus integration: implications for scaffold design and tissue engineering, Tissue Eng. 17 (1–2) (2011) 193–204.

[21] M.D. Brigham, A. Bick, E. Lo, A. Bendali, J.A. Burdick, A. Khademhosseini, Mechanically robust and bioadhesive collagen and photocrosslinkable hyaluronic acid semi-interpenetrating networks, Tissue Eng. 15 (7) (2009) 1645–1653.

[22] M.D. Lombardo, L. Mangiavini, G.M. Peretti, Biomaterials and meniscal lesions: current concepts and future perspective, Pharmaceutics 13 (11) (2021) 1886.

[23] S. Park, T.C. Laskow, J. Chen, P. Guha, B. Dawn, D.H. Kim, Microphysiological systems for human aging research, Aging Cell (2024) e14070.

[24] K.L. Xu, N. Di Caprio, H. Fallahi, M. Dehghany, M.D. Davidson, L. Laforest, B. C. Cheung, Y. Zhang, M. Wu, V. Shenoy, Microinterfaces in biopolymer-based bicontinuous hydrogels guide rapid 3D cell migration, Nat. Commun. 15 (1) (2024) 2766.

[25] M.B. Riffe, M.D. Davidson, G. Seymour, A.P. Dhand, M.E. Cooke, H.M. Zlotnick, R. R. McLeod, J.A. Burdick, Multi-material volumetric additive manufacturing of hydrogels using gelatin as a sacrificial network and 3D suspension bath, Adv. Mater. (2024) 2309026.

[26] I.E. Erickson, S.C. van Veen, S. Sengupta, S.R. Kestle, R.L. Mauck, Cartilage matrix formation by bovine mesenchymal stem cells in three-dimensional culture is age-dependent, Clin. Orthop. Relat. Res. 469 (10) (2011) 2744–2753.

[27] T.P. Driscoll, B.D. Cosgrove, S.-J. Heo, Z.E. Shurden, R.L. Mauck, Cytoskeletal to nuclear strain transfer regulates YAP signaling in mesenchymal stem cells, Biophys. J. 108 (12) (2015) 2783–2793.

[28] B. Yang, H. Sun, F. Song, M. Yu, Y. Wu, J. Wang, YAP1 negatively regulates chondrocyte differentiation partly by activating the β-catenin signaling pathway, Int. J. Biochem. Cell Biol. 87 (2017) 104–113.

[29] E. Öztürk, E. Despot-Slade, M. Pichler, M. Zenobi-Wong, RhoA activation and nuclearization marks loss of chondrocyte phenotype in crosstalk with Wnt pathway, Exp. Cell Res. 360 (2) (2017) 113–124.

[30] S. Dupont, L. Morsut, M. Aragona, E. Enzo, S. Giulitti, M. Cordenonsi, F. Zanconato, J. Le Digabel, M. Forcato, S. Bicciato, Role of YAP/TAZ in mechanotransduction, Nature 474 (7350) (2011) 179–183.

[31] W. Zhong, W. Zhang, S. Wang, J. Qin, Regulation of fibrochondrogenesis of mesenchymal stem cells in an integrated microfluidic platform embedded with biomimetic nanofibrous scaffolds, PLoS One 8 (4) (2013) e61283.

[32] A. Karystinou, A.J. Roelofs, A. Neve, F.P. Cantatore, H. Wackerhage, C. De Bari, Yes-associated protein (YAP) is a negative regulator of chondrogenesis in mesenchymal stem cells, Arthritis Res. Ther. 17 (2015) 1–14.

[33] W. Zhong, Y. Li, L. Li, W. Zhang, S. Wang, X. Zheng, YAP-mediated regulation of the chondrogenic phenotype in response to matrix elasticity, J. Mol. Histol. 44 (2013) 587–595.

[34] W. Zhong, K. Tian, X. Zheng, L. Li, W. Zhang, S. Wang, J. Qin, Mesenchymal stem cell and chondrocyte fates in a multishear microdevice are regulated by Yes-associated protein, Stem Cells Dev. 22 (14) (2013) 2083–2093.

[35] H. Alizadeh Sardroud, T. Wanlin, X. Chen, B.F. Eames, Cartilage tissue engineering approaches need to assess fibrocartilage when hydrogel constructs are mechanically loaded, Front. Bioeng. Biotechnol. 9 (2022) 787538.

[36] B. Huang, P. Li, M. Chen, L. Peng, X. Luo, G. Tian, H. Wang, L. Wu, Q. Tian, H. Li, Hydrogel composite scaffolds achieve recruitment and chondrogenesis in cartilage tissue engineering applications, J. Nanobiotechnol. 20 (1) (2022) 25.

[37] E. Folkesson, A. Turkiewicz, M. Rydén, H.V. Hughes, N. Ali, J. Tjörnstrand, P. Önnerfjord, M. Englund, Proteomic characterization of the normal human medial meniscus body using data-independent acquisition mass spectrometry, J. Orthop. Res. 38 (8) (2020) 1735–1745.

[38] H.-Y. Ma, Q. Li, W.R. Wong, E.-N. N'Diaye, P. Caplazi, H. Bender, Z. Huang, A. Arlantico, S. Jeet, A. Wong, LOXL4, but not LOXL2, is the critical determinant of pathological collagen cross-linking and fibrosis in the lung, Sci. Adv. 9 (21) (2023) eadf0133.

[39] W. Kong, C. Lyu, H. Liao, Y. Du, Collagen crosslinking: effect on structure, mechanics and fibrosis progression, Biomed. Mater. 16 (6) (2021) 062005.

[40] B.S. Spearman, N.K. Agrawal, A. Rubiano, C.S. Simmons, S. Mobini, C.E. Schmidt, Tunable methacrylated hyaluronic acid-based hydrogels as scaffolds for soft tissue engineering applications, J. Biomed. Mater. Res. 108 (2) (2020) 279–291.

[41] H. Kim, B. Kang, X. Cui, S.H. Lee, K. Lee, D.W. Cho, W. Hwang, T.B. Woodfield, K. S. Lim, J. Jang, Light-activated decellularized extracellular matrix-based bioinks for volumetric tissue analogs at the centimeter scale, Adv. Funct. Mater. 31 (32) (2021) 2011252.

[42] S. Ahn, U. Sharma, K.C. Kasuba, N. Strohmeyer, D.J. Müller, Engineered biomimetic fibrillar fibronectin matrices regulate cell adhesion initiation, migration, and proliferation via α5β1 integrin and syndecan-4 crosstalk, Adv. Sci. 10 (24) (2023) 2300812.

[43] J.A. Burdick, C. Chung, X. Jia, M.A. Randolph, R. Langer, Controlled degradation and mechanical behavior of photopolymerized hyaluronic acid networks, Biomacromolecules 6 (1) (2005) 386–391.

[44] S. Chae, S.-S. Lee, Y.-J. Choi, G. Gao, J.H. Wang, D.-W. Cho, 3D cell-printing of biocompatible and functional meniscus constructs using meniscus-derived bioink, Biomaterials 267 (2021) 120466.

[45] R.B. Brackin, G.E. McColgan, S.A. Pucha, M.A. Kowalski, H. Drissi, T.N. Doan, J. M. Patel, Improved cartilage protection with low molecular weight hyaluronic acid hydrogel, Bioengineering 10 (9) (2023) 1013.

[46] J. Jang, H.-J. Park, S.-W. Kim, H. Kim, J.Y. Park, S.J. Na, H.J. Kim, M.N. Park, S. H. Choi, S.H. Park, 3D printed complex tissue construct using stem cell-laden decellularized extracellular matrix bioinks for cardiac repair, Biomaterials 112 (2017) 264–274.

[47] F. Pati, J. Jang, D.-H. Ha, S. Won Kim, J.-W. Rhie, J.-H. Shim, D.-H. Kim, D.-W. Cho, Printing three-dimensional tissue analogues with decellularized extracellular matrix bioink, Nat. Commun. 5 (1) (2014) 3935.

[48] D. Szklarczyk, A. Franceschini, S. Wyder, K. Forslund, D. Heller, J. Huerta-Cepas, M. Simonovic, A. Roth, A. Santos, K.P. Tsafou, STRING v10: protein–protein interaction networks, integrated over the tree of life, Nucleic Acids Res. 43 (D1) (2015) D447–D452.

[49] P. Shannon, A. Markiel, O. Ozier, N.S. Baliga, J.T. Wang, D. Ramage, N. Amin, B. Schwikowski, T. Ideker, Cytoscape: a software environment for integrated models of biomolecular interaction networks, Genome Res. 13 (11) (2003) 2498–2504.

[50] D.H. Kim, J.T. Martin, D.M. Elliott, L.J. Smith, R.L. Mauck, Phenotypic stability, matrix elaboration and functional maturation of nucleus pulposus cells encapsulated in photocrosslinkable hyaluronic acid hydrogels, Acta Biomater. 12 (2015) 21–29.

[51] M. Guvendiren, J.A. Burdick, Stiffening hydrogels to probe short-and long-term cellular responses to dynamic mechanics, Nat. Commun. 3 (1) (2012) 792.

[52] V.G. Muir, M. Fainor, B.S. Orozco, R.L. Hilliard, M. Boyes, H.E. Smith, R.L. Mauck, T.P. Schaer, J.A. Burdick, S.E. Gullbrand, Injectable radiopaque hyaluronic acid granular hydrogels for intervertebral disc repair, Adv. Healthcare Mater. (2023) 2303326.

[53] K.H. Song, S.J. Heo, A.P. Peredo, M.D. Davidson, R.L. Mauck, J.A. Burdick, Influence of fiber stiffness on meniscal cell migration into dense fibrous networks, Adv. Healthcare Mater. 9 (8) (2020) 1901228.

[54] A.H. Huang, A. Stein, R.S. Tuan, R.L. Mauck, Transient exposure to transforming growth factor beta 3 improves the mechanical properties of mesenchymal stem cell–laden cartilage constructs in a density-dependent manner, Tissue Eng. 15 (11) (2009) 3461–3472.

[55] S.-J. Heo, W.M. Han, S.E. Szczesny, B.D. Cosgrove, D.M. Elliott, D.A. Lee, R. L. Duncan, R.L. Mauck, Mechanically induced chromatin condensation requires cellular contractility in mesenchymal stem cells, Biophys. J. 111 (4) (2016) 864–874.

[56] R. Mauck, X. Yuan, R.S. Tuan, Chondrogenic differentiation and functional maturation of bovine mesenchymal stem cells in long-term agarose culture, Osteoarthr. Cartil. 14 (2) (2006) 179–189.

[57] S. Tarafder, G. Park, C.H. Lee, Explant models for meniscus metabolism, injury, repair, and healing, Connect. Tissue Res. 61 (3–4) (2020) 292–303.